Optical approaches to improving perovskite/Si tandem cells

Haejun Chung[1], Xingshu Sun[1], and Peter Bermel[1]
[1]Birck Nanotechnology Center, Electrical and Computer Engineering, 1205 W. State St, West Lafayette, IN 47906, U.S.A.

ABSTRACT
Recently, metal-halide perovskites have demonstrated an extraordinarily rapid advance in single junction cell efficiency to over 20%, while still offering potentially low costs. Since the bandgap is larger than the ideal single-junction value, perovskite-based tandem cells can theoretically offer even higher efficiencies. Instead, however, the record tandem cell performance in experiments to date has come in slightly below that of record single junctions, although slightly higher than the same single junctions. In this work, we consider both how this disconnect can be explained quantitatively, and then devise experimentally feasible, variance-aware approaches to address them. The first stage of our approach is based on reconfiguring dielectric front coatings to help reduce net reflected power and balance junction currents by reshaping the reflection peaks. This method could be applied to post-fabrication stage of perovskite/c-Si tandem cells, and also applicable to cell and module level structures. In the second stage of our approach, we can almost entirely eliminate Fresnel reflection by applying a conformal periodic light trapping structure. In the best case, a short circuit current (J_{sc}) of 18.0 mA/cm^2 was achieved, after accounting for 4.8 mA/cm^2 of parasitic loss and 1.6 mA/cm^2 reflection loss. Further improvements may require a change in the baseline materials used in perovskite cells.

INTRODUCTION
Metal-halide perovskites have gained a great deal of attention for their extraordinarily rapid increase in single junction efficiencies, rising from below 1% to now exceeding 20 % [1,2]. Furthermore, perovskites are solution-processable materials that appear resilient in the presence of defects [1,2]; thus, they have a potential to serve as ultra-low cost solar cells. Although long-term stability and reliability is a major potential challenge, recent work has suggested these problems could be addressed successfully [3]. Furthermore, metal-halide perovskites have a

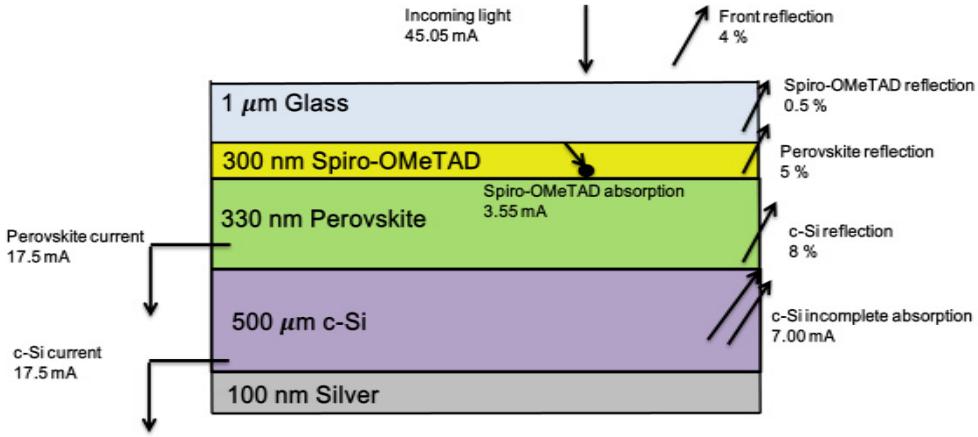

Fig. 1: Schematic diagram representing average reflection and parasitic absorption losses in perovskite/silicon tandem cells. The average reflection was calculated by Fresnel's law (without accounting for multiple reflections here).

large and tunable bandgap, which raises the prospects of even higher efficiencies as a top cell in a tandem solar cell. Recently, perovskite-crystalline silicon tandem cells were proposed, with theoretical efficiencies expected to exceed 30 % [4–6]. However, measured efficiencies more typically fall between 13% and 18 %, which is below that [5,7–9]. Reaching this theoretical limits is still challenging for a variety of reasons. First, the hole transport layers (HTL) for perovskites are not transparent enough for visible and infrared wavelengths [10]. For example, Spiro-OMeTAD shows excellent hole-collecting efficiency, but suffers nearly 10% parasitic losses at the most commonly employed thicknesses of around several hundred nanometers. In single junction perovskites, Spiro-OMeTAD parasitic loss is less important, because it is usually deposited at the back side. In a tandem configuration, it may absorb many more photons when it is placed at the intermediate layer between top and bottom junctions, or top window layer. Recently, PEDOT:PSS [11,12] was suggested as a window layer of perovskites, but its charge collection efficiency was not comparable to Spiro-OMeTAD. The other challenge in this tandem configuration is mismatched bandgaps. Bottom junctions made of crystalline silicon require top junctions with bandgaps of 1.7-1.8 eV for highest performance. In other words, 1.55 eV metal-halide perovskites may suffer slight open-circuit voltage loss, as well as short-circuit current mismatch. Thus, many optical studies have been performed to predict the optimum perovskite thickness for matched junction current [13–15]. However, there has been no clear agreement among these studies. It is natural, because perovskites are typically unstable as photovoltaic materials [16], which cause significant performance variations both between and within samples made through the same manufacturing process [17]. Finally, current perovskite/c-Si tandem designs may suffer non-trivial reflection losses to large refractive index contrast among the layers. The average reflectivity among the layers are shown in Fig. 1. Even though perovskite/c-Si tandem cells may suffer substantial reflection losses, conventional light trapping may not help, as it may increase the HTL parasitic loss simultaneously.

In this study, we propose front coatings which potentially can solve both problems, short-circuit mismatch and non-trivial amount of total reflection occurring in the experimental cells. Next, light trapping approach will be applied for a further performance enhancement with considering HTL parasitic loss.

THEORY

Conventional anti-reflection coatings (ARC) for photovoltaic cells are designed to target the intensity peak of the AM1.5 solar spectrum, which is around 550 nm [18]. Thus, the design rule is simply given by the quarter-wave condition. As shown Fig. 2, thicker ARCs can have a red-shifted reflection minimum. This implies that controlling the effective ARC thickness may affect the tandem cell junction current. Although well-designed conventional tandem solar cells (e.g., micromorph silicon tandem, III-V tandems) should not have significant current mismatch, thus a typical quarter-wave ARC design targeting ~550 nm is preferred. However, in the current early stage of experimental monolithic perovskite/silicon tandem cells, significant short circuit current mismatches have been reported [5] as well as external quantum efficiency degradation in the perovskite junction [9]. These often originate from the intrinsic instability of perovskite materials. For example, perovskite solar cells show a performance variation under different measured time, and these cells also have well-known light soaking degradation and humidity exposure degradation. The unstable characteristics of perovskite materials make current matching of perovskite-based tandem cells very challenging. In this work, we employ a front

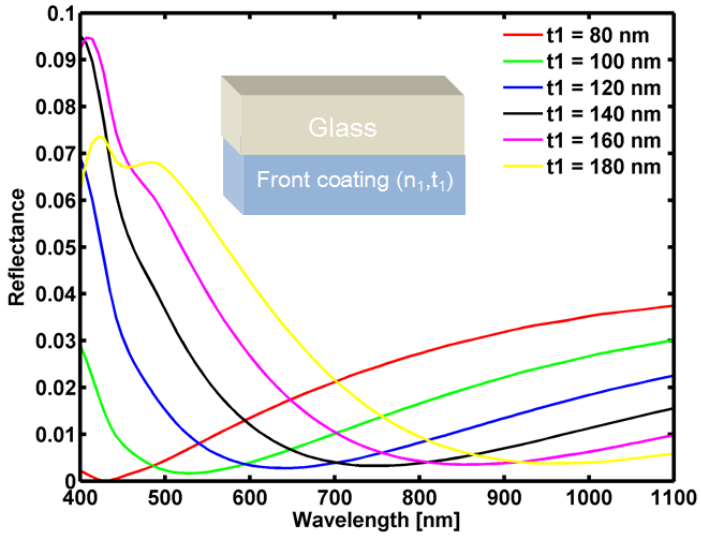

Fig. 2: Reflectance calculation by Fresnel's law. The green and red curves are similar to the conventional anti-reflection coating for silicon solar cells while this work utilizes tuning in the reflectance minimum that is shown in this Figure. The inset shows the calculated structure. The refractive index was assume to 1.35.

coating control method to re-balance mismatched short circuit current in this tandem design, which can be applied after a fabrication process of the tandem cell.

To examine this phenomenon and quantify its benefits, we employ a full-wave optical simulation using Finite Difference Time Domain (FDTD) method. FDTD has been widely used in previous photovoltaic simulations. However, in the FDTD method, simulating newly developed photovoltaic materials (e.g., perovskites, CdTe etc.) were challenging due to the difficulty of developing a time domain dispersion model for them. Recently, the present authors have demonstrated a quadratic complex rational function (QCRF) model [19,20] for photovoltaic materials [21,22], thus in this work, we employ QCRF based FDTD method for a full-wave optical simulation (400 ~ 1200 nm) of perovskite/silicon tandem cells. To simulate a wafer-based c-Si in FDTD, we measure the absorption of a 2 micron-thick c-Si cell within a tandem cell, and then analytically extend to a larger thickness in the following manner. First, the effective absorption coefficient for the c-Si structure at each wavelength is calculated from the absolute absorption in FDTD as follows:

$$\mathrm{A_{sim}} = 1 - e^{-\alpha t_{sim}} \simeq 1 - \left(1 - \alpha t_{sim} + \frac{\alpha^2 t_{sim}^2}{2!} + \cdots\right),$$

where $\mathrm{A_{sim}}$ indicates absorption calculated by the FDTD simulation, α is an absorption coefficient for the tandem simulation, t_{sim} is a c-Si thickness for the simulation which was set to 2 microns. Then, wafer-based silicon cells are approximated by:

$$\mathrm{A_{wafer}} \simeq (1 - e^{-\alpha t_{wafer}}) * T_{si},$$

where A_{wafer} indicates a wafer based c-Si layer absorption, t_{wafer} is a c-Si wafer thickness for the approximation which was set in 500 microns in this study, and T_{si} is the transmittance calculated at the boundary of perovskite and silicon layers. The absorption calculated by FDTD is then used to predict the short circuit current density (J_{sc}):

$$J_{sc} = \int_0^{\infty} d\lambda \left[\frac{e\lambda}{hc}\frac{dI}{d\lambda}A(\lambda)\right],$$

where $\frac{dI}{d\lambda}$ indicates the solar spectrum given by AM1.5G, and $A(\lambda)$ represents the partial absorption of active layer calculated under short circuit conditions. Note that this formulation assumes ideal collection of generated carriers [i.e., IQE(λ)=1 for $\lambda < \lambda_g$].

DISCUSSION

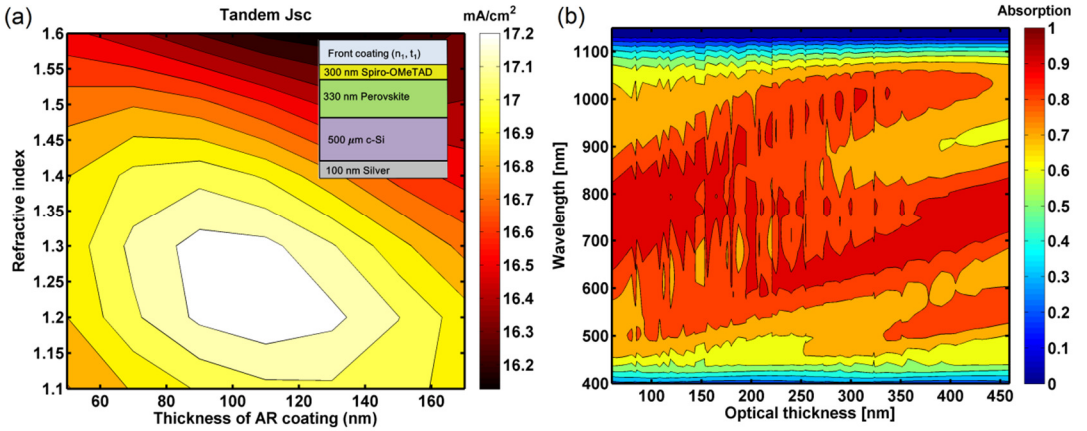

Fig. 3: (a) Single-layer front coating optimization for 330 nm-thick perovskite case. The optimum was found when n_1 = 1.3, t_1 = 100 nm. (b) Absorption spectrum for different optical thicknesses ($n_1 \times t_1$). Three modes are observed, each corresponding to an impedance match with the PV active material region.

First, we study a cell level perovskite/silicon structure, which includes a single layer of a front coating on top of the HTL; in contrast, a module level structure typically has a glass layer on top of a front coating. The electromagnetic flux monitors were inserted at the boundary of absorptive materials (Spiro-OMeTAD, perovskite, c-Si and silver) to calculate partial absorption. Now, we vary refractive index and thickness of the front coating to optimize it. Fig. 3(a) shows that the optimized front coating (n_1 = 1.3, t_1 = 100 nm) is very close to the theoretical quarter-wave ARC design of the previous section. The absorption spectrum for this optimization are plotted in Fig. 3(b). Three absorption modes are observed along varying optical thickness of a front coating.

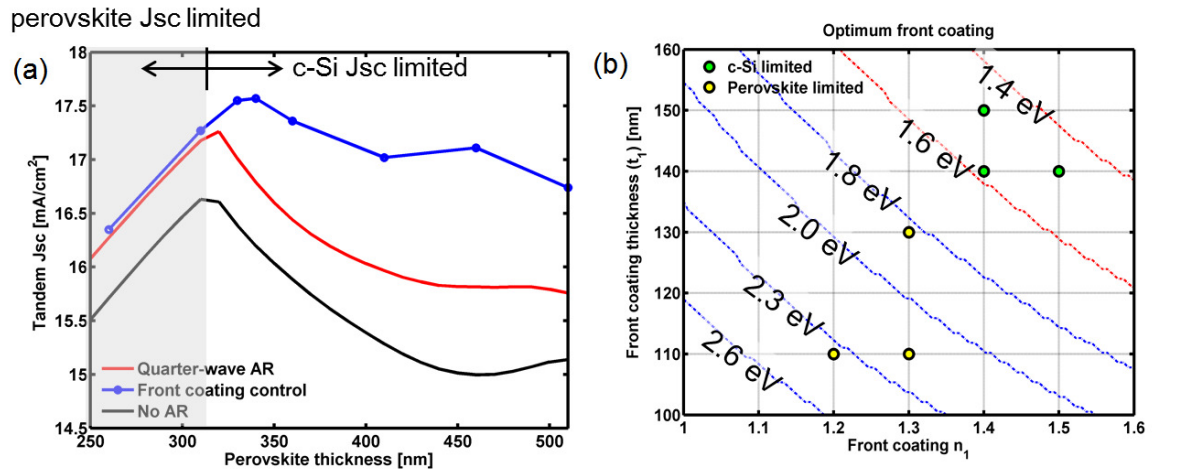

Fig. 4: (a) The ideal quarter-wave AR coating (red curve) can have slight J_{sc} enhancement while the proposed front coating method (blue curve) can have a J_{sc} enhancement over a broader range of c-Si limited cases. (b) The optimum front coatings for each optimized data point. Dashed lines represent

Similarly, we optimize the front coatings for different perovskite thicknesses, which could be potentially interpreted as a perovskite short circuit current variation. As shown in Fig. 4(a), the front coating control can have meaningful gains in c-Si limited cases, while perovskite limited cases nearly have no benefit. This is mainly because the reference result already has a customized front coating for targeting a wavelength around 550 nm. The maximum gain found in this optimization was 1.8 mA/cm^2 in tandem J_{sc}. This improvement could be meaningful, because tandem solar cells generally have a larger open circuit voltage which will be multiplied by matched J_{sc} to calculate cell efficiency. As shown in Fig. 4. (b), the optimized front coatings are determined by Fresnel's law. The perovskite-limited cases require smaller optical thicknesses than the conventional 550-nm-targeted ARC, while the c-Si limited cases require a larger optical

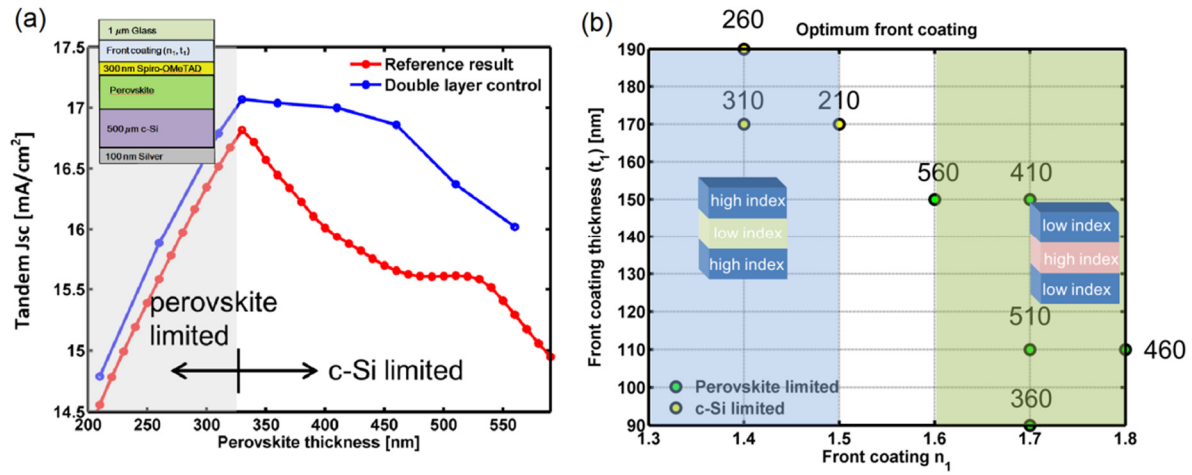

Fig. 5: (a) The ideal quarter-wave AR coating (red curve) can have slight J_{sc} enhancement,while the proposed front coating method (blue curve) can have a J_{sc} enhancement over a broader range of c-Si limited cases. (b) The optimum front coating thicknesses for a range of front coating indices (perovskite thickness is indicated as a number above each circle). Since the Spiro-OMETAD has n=1.55, crossing this value flips the effective ordering of layer indices.

thicknesses.

Now we consider more realistic module level designs which include a mechanically robust SiO_2 layer. Generally, it is very essential for perovskite based solar cells to have an anti-humidity encapsulant at the exterior, because they are very volatile to H_2O exposure. The front glass could be several hundred microns to several hundred millimeters, but in this simulation, we assume that the front glass is one micron which could be enough to see an optical response of the solar modules. The front coating is now placed between glass and Spiro-OMeTAD. The refractive index contrast between glass and Spiro-OMeTAD is very trivial, so the Fresnel reflection does not exceed 1 %. Fig. 5(a) shows the optimization results, calculated similarly to the cell level optimizations. Interestingly, perovskite limited cases do not have a significant benefit from the proposed method, while the c-Si limited cases show meaningful Jsc gains. This is mainly because Fresnel reflection among the layers are occurring in longer wavelengths as observed in the experiment [5,9], thus adjusting the target wavelengths of a front coating to lower wavelength regime may not be very beneficial. Fig. 5(b) shows the optimized front coatings for two biased cases. Unlike the previous cell level optimization, the module level structure is no longer governed by a simple quarter wave design. For example, in the perovskite limited cases, the optimum front coatings have lower or similar refractive index from its neighborhood layers while, in the opposite cases, the optimum front coatings are found in high refractive index regime. The maximum J_{sc} gain in this method, as denoted double layer control, 1.8 mA/cm^2 when the perovskite layer is 460-nm-thick. This implies that c-Si limited tandem cells could have much benefit from the front coating control method, which might be a typical case for a planar perovskite/silicon tandem structure because an intrinsic c-Si has an indirect bandgap causing incomplete absorption in NIR regime. Using the measured open circuit voltage and fill factor for experimental tandem cells [9], this J_{sc} enhancement corresponds to a significant 2.47% absolute efficiency enhancement.

Finally, we consider 3D periodic light trapping schemes for perovskite/silicon tandem cells. As shown in an inset of Fig. 6(a), honeycomb-type conformal texturing is applied here. The c-Si junction current is enhanced by increasing the periodicity of the texturing (since it traps longer wavelengths). On the other hand, the perovskite current is slightly decreased, which could

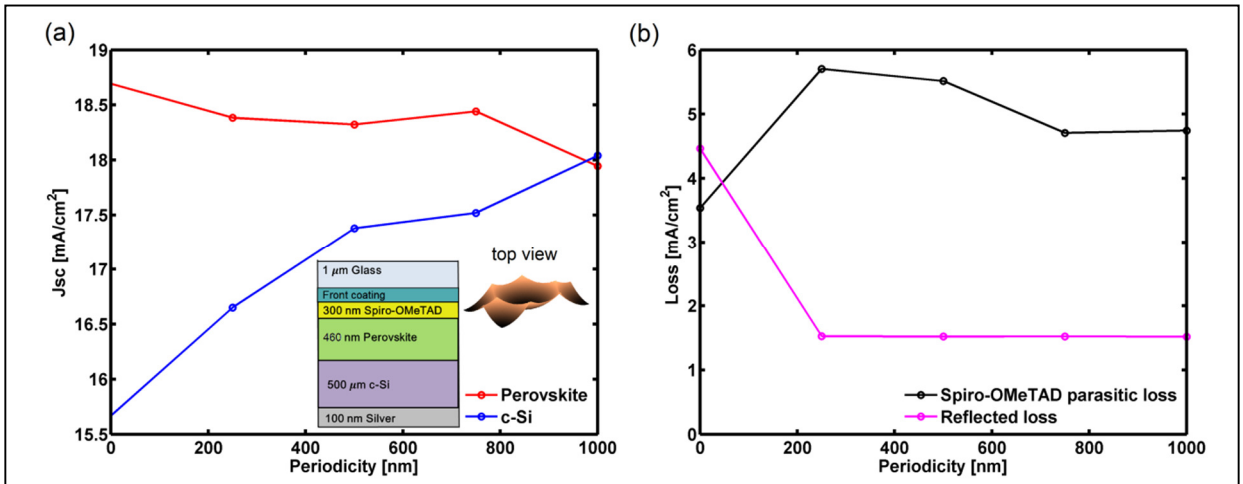

Fig. 6: (a) Light trapping results for perovskite/silicon tandem cells for a system with an initial excess of perovskite current. The inset shows the simulation geometry. This shows that light trapping can bridge a short current gap of 3 mA/cm^2; (b) parasitic and reflection losses with increasing light trapping.

initially seem counterintuitive. There are two main reasons for this phenomenon. First, the applied light trapping increases Spiro-OMeTAD parasitic absorption; thus, the number of transmitted photon in the perovskite layer is decreased. Second, Fresnel's reflection between perovskite and c-Si layers is eliminated in the light trapping structure, resulting complete single-pass absorption in the perovskite layer. Thus, applying light trapping to perovskite/silicon tandem cells do not necessarily increase top junction current. The maximum short circuit current density demonstrated in this conformal periodic light trapping was 18 mA/cm^2, which is nearly $1mA/cm^2$ gain from the front layer control method. In order to further increase J_{sc} by light trapping, Spiro-OMeTAD parasitic absorption should be suppressed. As an alternative light trapping strategy, plasmonic light trapping [23,24] and dielectric back grating [25,26] could be applied to minimize Spiro-OMeTAD absorption while increasing c-Si light trapping,

CONCLUSIONS

In conclusion, this work has shown optical approaches to re-design reflection peaks for solving current matching problems in perovskite/silicon tandem cells, which are non-trivial problems due to mismatched bandgaps, variability, and degradation of perovskite materials. Cell level tandem structures can have 1.2 mA/cm^2 J_{sc} enhancement in c-Si limited cases, while module level tandem structures can have 1.8 mA/cm^2 J_{sc} gains in the same cases. Finally, periodic conformal light trappings have been applied to eliminate Fresnel reflections among the layers. This approach yields an additional 1 mA/cm^2 J_{sc} enhancement from the front layer control method. The total efficiency in this case can be 24.4% if we use the best Voc and FF from prior tandem cells, or 29.8 % if we combine the best Voc and FF from individual single-junction perovskite and silicon cells. This result suggests that a perovskite-silicon tandem with efficiency higher than the world-record single junction perovskite cell is very well within reach for an enterprising experimental research group.

ACKNOWLEDGMENTS

The authors thank Prof. A. Alam for valuable discussions. Support was provided by the Department of Energy, under DOE Cooperative Agreement No. DE-EE0004946 (PVMI Bay Area PV Consortium), the Semiconductor Research Corporation, under Research Task No. 2110.006 (Network for Photovoltaic Technologies), the National Science Foundation, under Award EEC1454315-CAREER: Thermophotonics for Efficient Harvesting of Waste Heat as Electricity.

REFERENCES

1. H.-S. Kim, C.-R. Lee, J.-H. Im, K.-B. Lee, T. Moehl, A. Marchioro, S.-J. Moon, R. Humphry-Baker, J.-H. Yum, J. E. Moser, M. Grätzel, and N.-G. Park, "Lead iodide perovskite sensitized all-solid-state submicron thin film mesoscopic solar cell with efficiency exceeding 9%.," Sci. Rep. **2**, 591 (2012).

2. M. M. Lee, J. Teuscher, T. Miyasaka, T. N. Murakami, and H. J. Snaith, "Efficient hybrid solar cells based on meso-superstructured organometal halide perovskites.," Science **338**, 643–7 (2012).

3. H. Zhou, Q. Chen, G. Li, S. Luo, T. -b. Song, H.-S. Duan, Z. Hong, J. You, Y. Liu, and Y. Yang, "Interface engineering of highly efficient perovskite solar cells," Science (80-.). **345**, 542–546 (2014).

4. I. Almansouri, A. Ho-Baillie, and M. A. Green, "Ultimate efficiency limit of single-junction perovskite and dual-junction perovskite/silicon two-terminal devices," Jpn. J. Appl. Phys. **54**, 08KD04 (2015).

5. J. P. Mailoa, C. D. Bailie, E. C. Johlin, E. T. Hoke, A. J. Akey, W. H. Nguyen, M. D. McGehee, and T. Buonassisi, "A 2-terminal perovskite/silicon multijunction solar cell enabled by a silicon tunnel junction," Appl. Phys. Lett. **106**, 121105 (2015).

6. R. Asadpour, R. V. K. Chavali, M. Ryyan Khan, and M. A. Alam, "Bifacial Si heterojunction-perovskite organic-inorganic tandem to produce highly efficient ($\eta T^* \sim 33\%$) solar cell," Appl. Phys. Lett. **106**, 243902 (2015).

7. P. Löper, S.-J. Moon, S. M. de Nicolas, B. Niesen, M. Ledinsky, S. Nicolay, J. Bailat, J.-H. Yum, S. De Wolf, and C. Ballif, "Organic-inorganic halide perovskite/crystalline silicon four-terminal tandem solar cells.," Phys. Chem. Chem. Phys. **17**, 1619–29 (2015).

8. C. D. Bailie, M. G. Christoforo, J. P. Mailoa, A. R. Bowring, E. L. Unger, W. H. Nguyen, J. burschka, N. Pellet, J. Z. Lee, M. Grätzel, R. Noufi, T. Buonassisi, A. Salleo, and M. D. McGehee, "Polycrystalline Tandem Photovoltaics Using Perovskites on Top of Silicon and CIGS," Energy Environ. Sci. **8**, 956–963 (2014).

9. S. Albrecht, M. Saliba, J. P. Correa Baena, F. Lang, L. Kegelmann, M. Mews, L. Steier, A. Abate, J. Rappich, L. Korte, R. Schlatmann, N. Mohammad K., A. Hagfeldt, M. Grätzel, and B. Rech, "Monolithic Perovskite/Silicon-Heterojunction Tandem Solar Cells Processed at Low Temperature," Energy Environ. Sci. (2015).

10. W. H. Nguyen, C. D. Bailie, E. L. Unger, and M. D. McGehee, "Enhancing the Hole-Conductivity of Spiro-OMeTAD without Oxygen or Lithium Salts by Using Spiro(TFSI) 2 in Perovskite and Dye-Sensitized Solar Cells," J. Am. Chem. Soc. **136**, 10996–11001 (2014).

11. O. Malinkiewicz, A. Yella, Y. H. Lee, G. M. Espallargas, M. Graetzel, M. K. Nazeeruddin, and H. J. Bolink, "Perovskite solar cells employing organic charge-transport layers," Nat. Photonics **8**, 128–132 (2013).

12. J. Liu, S. Pathak, T. Stergiopoulos, T. Leijtens, K. Wojciechowski, S. Schumann, N. Kausch-Busies, and H. J. Snaith, "Employing PEDOT as the p-Type Charge Collection Layer in Regular Organic-Inorganic Perovskite Solar Cells.," J. Phys. Chem. Lett. **6**, 1666–73 (2015).

13. M. Filipič, P. Löper, B. Niesen, S. De Wolf, J. Krč, C. Ballif, and M. Topič, "CH(3)NH(3)PbI(3) perovskite / silicon tandem solar cells: characterization based optical simulations.," Opt. Express **23**, A263–78 (2015).

14. N. N. Lal, T. P. White, and K. R. Catchpole, "Optics and Light Trapping for Tandem Solar Cells on Silicon," IEEE J. Photovoltaics **4**, 1380–1386 (2014).

15. B. W. Schneider, N. N. Lal, S. Baker-Finch, and T. P. White, "Pyramidal surface textures for light trapping and antireflection in perovskite-on-silicon tandem solar cells.," Opt. Express **22**, A1422–30 (2014).

16. K. Wojciechowski, M. Saliba, T. Leijtens, A. Abate, and H. J. Snaith, "Sub-150 °C processed meso-superstructured perovskite solar cells with enhanced efficiency," Energy Environ. Sci. **7**, 1142–1147 (2014).

17. Y. Chen, T. Chen, and L. Dai, "Layer-by-layer growth of CH_3 NH_3 PbI(3-x)Clx for highly efficient planar heterojunction perovskite solar cells.," Adv. Mater. **27**, 1053–9 (2015).

18. J. Zhao and M. A. Green, "Optimized antireflection coatings for high-efficiency silicon solar cells," IEEE Trans. Electron Devices **38**, 1925–1934 (1991).

19. H. Chung, "Accurate FDTD Dispersive Modeling for Concrete Materials," ETRI J. **35**, 915–918 (2013).

20. S.-G. Ha, J. Cho, J. Choi, H. Kim, and K.-Y. Jung, "FDTD Dispersive Modeling of Human Tissues Based on Quadratic Complex Rational Function," IEEE Trans. Antennas Propag. **61**, 996–999 (2013).

21. H. Chung, K.-Y. Jung, X. T. Tee, and P. Bermel, "Time domain simulation of tandem silicon solar cells with optimal textured light trapping enabled by the quadratic complex rational function.," Opt. Express **22**, A818–32 (2014).

22. H. Chung, S.-G. Ha, J. Choi, and K.-Y. Jung, "Accurate FDTD modelling for dispersive media using rational function and particle swarm optimisation," Int. J. Electron. **102**, 1218–1228 (2014).

23. H. Chung, K.-Y. Jung, and P. Bermel, "Flexible flux plane simulations of parasitic absorption in nanoplasmonic thin-film silicon solar cells," Opt. Mater. Express **5**, 2054 (2015).

24. V. E. Ferry, M. A. Verschuuren, H. B. T. Li, E. Verhagen, R. J. Walters, R. E. I. Schropp, H. A. Atwater, and A. Polman, "Light trapping in ultrathin plasmonic solar cells.," Opt. Express **18**, A237–A245 (2010).

25. P. Bermel, C. Luo, L. Zeng, L. C. Kimerling, and J. D. Joannopoulos, "Improving thin-film crystalline silicon solar cell efficiencies with photonic crystals," Opt. Express **15**, 16986 (2007).

26. D. Zhou and R. Biswas, "Photonic crystal enhanced light-trapping in thin film solar cells," J. Appl. Phys. **103**, 093102 (2008).